EVALUATION OF CONVEX HULL METHODS TO PREDICT EQUIVALENT STRESSES IN MULTIAXIAL FATIGUE

Marco Antonio Meggiolaro, meggi@puc-rio.br
Jaime Tupiassú Pinho de Castro, jtcastro@puc-rio.br
Mechanical Engineering Department, PUC-Rio, Brasil

Abstract. *A critical issue in multiaxial fatigue damage calculation is how to find the equivalent stress or strain ranges and mean components associated with non-proportional (NP) histories. A traditional way to find such ranges is to use convex hull methods, which search for convex enclosures of the entire history path in stress or strain diagrams. In this work, all existing convex hull methods are presented and compared using results from more than $3x10^6$ Monte Carlo simulations of random and especially chosen path topologies in two to five-dimensional stress or strain diagrams. New convex hull models are also proposed, based on Deperrois' idea of longest chords. It is found that the proposed models are very similar to the Maximum Prismatic Hull model, but with a much simpler and efficient algorithm to compute equivalent stresses. It is also shown that the Minimum Circumscribed Ellipsoid, Minimum Volume Ellipsoid, and Minimum Ball (MB) methods may result in very poor predictions of the stress or strain amplitudes. The only recommended convex hull method based on ellipsoids is the Minimum F-norm Ellipsoid (MFE) which, together with the Maximum Prismatic Hull model and its variations, are very efficient to predict equivalent amplitudes in NP histories.*

Keywords: *multiaxial fatigue, equivalent stress, convex hull*

1. INTRODUCTION

Non-proportional (NP) multiaxial fatigue damage occurs when the principal stress directions vary during the loading induced by several independent sources, such as out-of-phase bending and torsion moments (Socie, 1999). Multiaxial fatigue damage models are based on stress or strain ranges. It is not difficult to define these ranges for constant amplitude loadings, where only two stress or strain states need to be considered, for the peak and the valley.

However, for multiaxial variable amplitude (VA) loadings, in special when the history is non-proportional (NP), it is not clear how these ranges should be defined and identified. The loading path, represented e.g. in the Mises diagram $\varepsilon \times \gamma/\sqrt{3}$, could have a generic curved shape spanning infinitely many strain states, without a clear peak or valley. A peak (or valley) of one strain component may not coincide with the peak (or valley) of the other strain components (Langlais et al., 2003). The following sections deal with how to quantify the stress or strain ranges used by the various multiaxial damage models, associated with VA-NP histories that are periodic in time.

Consider that the periodic history is formed by repeatedly following a given loading path domain $\boldsymbol{D}$, where $\boldsymbol{D}$ contains all points from the stress or strain variations along one period of the history. For a complex-shaped history such as the one shown in Fig. 1, it is not easy to decide how to obtain the effective $\Delta\tau_{max}$. The so-called convex hull methods try to find circles, ellipses or rectangles that contain the entire path (in the 2D case). In a nutshell, in the 2D case, the Minimum Ball (MB) method (Dang Van and Papadopoulos, 1999) searches for the circle with minimum radius that contains $\boldsymbol{D}$; the minimum ellipse methods (Freitas et al., 2000; Gonçalves et al., 2005; Zouain et al., 2006) search for an ellipse with semi-axes a and b that contains $\boldsymbol{D}$ with minimum area $\pi \cdot a \cdot b$ or minimum norm $(a^2 + b^2)^{1/2}$; and the maximum prismatic hull methods (Gonçalves et al., 2005; Mamiya et al., 2009) search among the smallest rectangles that contain $\boldsymbol{D}$ the one with maximum area or maximum diagonal (it's a max-min search problem). The value of $\Delta\tau_{max}$ in Fig. 1 would either be assumed as the value of the circle diameter, or twice the ellipse norm, or the rectangle diagonal. If the history path were represented in a $\gamma_B \times \gamma_{B2}$ diagram, the same methods would result $\Delta\gamma_{max}$ estimates.

The convex hull methods can also be applied to traction-torsion histories, if a $\sigma_x \times \tau_{xy}\sqrt{3}$ diagram is considered. The effective range in this case is the Mises stress range $\Delta\sigma_{Mises}$, defined in the next section. Similarly, for traction-torsion histories where plastic strains dominate, a strain diagram $\varepsilon_x \times \gamma_{xy}/\sqrt{3}$ can be used to predict an effective $\Delta\varepsilon_{Mises}$.

Such convex hull methods can be extended to histories involving more than two stress or strain components. E.g., if the history path is plotted in a 3D diagram representing 3 stress or strain components, the convex hull methods will search for spheres, ellipsoids or rectangular prisms. For higher dimension diagrams, the search is for hyperspheres, hyperellipsoids, and rectangular hyperprisms. However, this practice can lead to significant errors, since each convex hull will reflect an effective range calculated on different planes at different points in time. The recommended approach for general 6D histories involving all stress (or strain) components is then to project them onto Case A and Case B candidate planes (see Fig. 2), resulting in each case in searches for effective ranges in 2D diagrams $\sigma \times \tau\sqrt{3}$, $\varepsilon \times \gamma/\sqrt{3}$, $\tau_B \times \tau_{B2}$, or $\gamma_B \times \gamma_{B2}$.

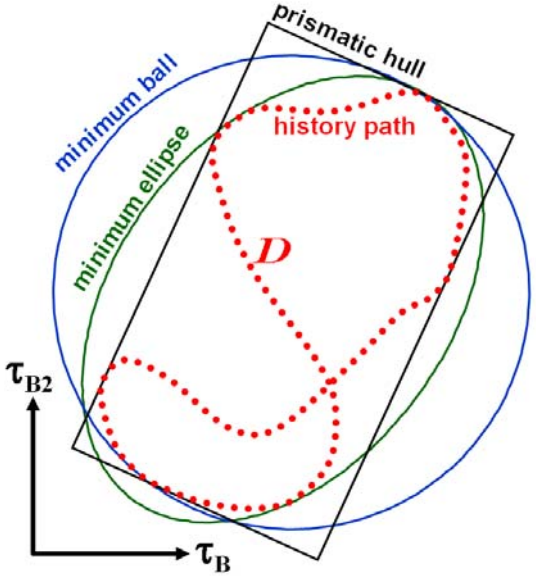

Fig. 1: Stress history path $\boldsymbol{D}$ in the $\tau_B \times \tau_{B2}$ diagram, enclosed in convex hulls based on circles (balls), ellipses and rectangular prisms.

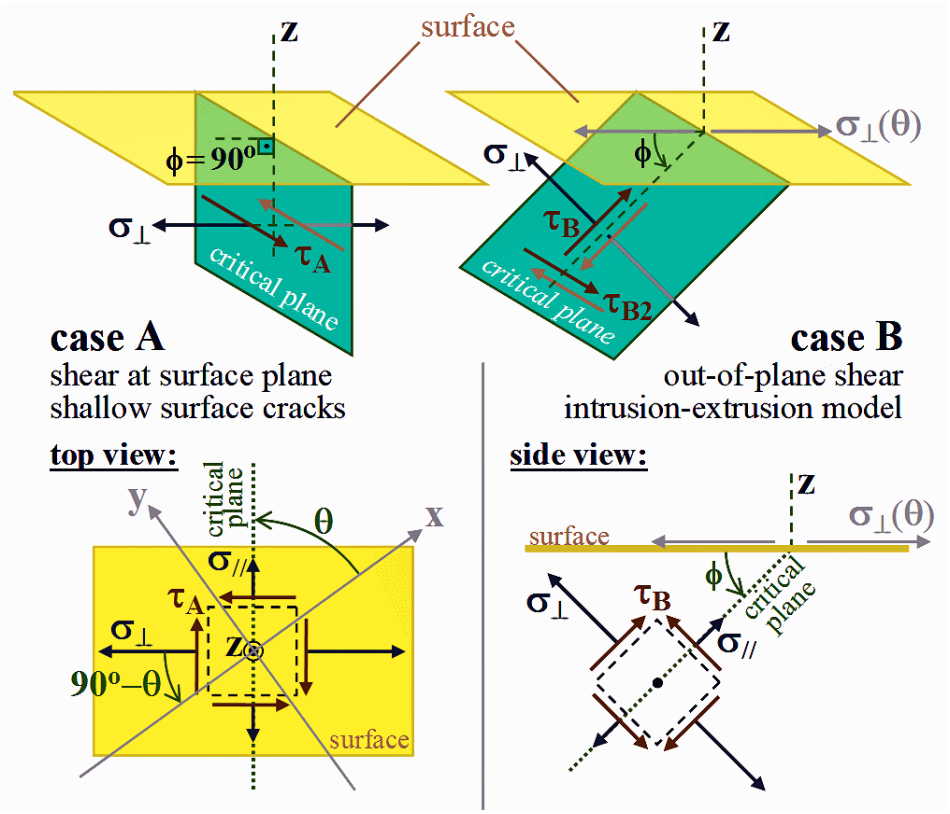

Fig. 2: Case A and Case B cracks.

The convex hull methods are described in detail in the following sections. Their framework is based on deviatoric stress (or strain) diagrams and Mises stress (or strain) parameters, which are discussed next.

2. MISES STRESS AND STRAIN PARAMETERS

The methods to obtain effective (or equivalent) stress and strain ranges usually make use of stress and strain parameters based on the Mises yield function. For linear elastic histories, both Mises effective stress σ_{Mises} and Mises (or octahedral) shear stress τ_{Mises} can be used as auxiliary parameters, where

$$\sigma_{Mises} = \frac{3}{\sqrt{2}}\tau_{Mises} = \frac{1}{\sqrt{2}}\sqrt{(\sigma_x-\sigma_y)^2+(\sigma_y-\sigma_z)^2+(\sigma_x-\sigma_z)^2+6(\tau_{xy}^2+\tau_{yz}^2+\tau_{xz}^2)} \quad (1)$$

Since the Mises stress σ_{Mises} (as well as the octahedral shear stress τ_{Mises}) equation is always positive, a Mises stress range $\Delta\sigma_{Mises}$ (also known as relative Mises stress σ_{RMises}) should be used to correctly evaluate the variation of σ_{Mises} due to a change $(\Delta\sigma_x, \Delta\sigma_y, \Delta\sigma_z, \Delta\tau_{xy}, \Delta\tau_{xz}, \Delta\tau_{yz})$ in the stress components along some loading path Δ:

$$\Delta\sigma_{Mises} = \sigma_{RMises} = \frac{\sqrt{(\Delta\sigma_x-\Delta\sigma_y)^2+(\Delta\sigma_x-\Delta\sigma_z)^2+(\Delta\sigma_y-\Delta\sigma_z)^2+6(\Delta\tau_{xy}^2+\Delta\tau_{xz}^2+\Delta\tau_{yz}^2)}}{\sqrt{2}} \quad (2)$$

Note that the Mises stress range correlates with the octahedral shear range parameter $\Delta\tau_{Mises}$, used in both Sines and Crossland models, through $\Delta\sigma_{Mises} = \Delta\tau_{Mises} \cdot 3/\sqrt{2}$.

The Mises effective strain ε_{Mises} is another useful quantity in VA-NP histories, in special to deal with plastic strains. It uses the mean or effective Poisson coefficient $\bar{\nu} = (0.5\varepsilon_{pl} + \nu_{el}\varepsilon_{el})/(\varepsilon_{pl} + \varepsilon_{el})$ to include plastic effects, where ε_{el} and ε_{pl} are the elastic and plastic components of the strains, and ν_{el} and ν_{pl} are the elastic and plastic Poisson coefficients (where $\nu_{pl} = 0.5$). The Mises strain correlates with the octahedral (or Mises) shear strain γ_{Mises}, which is the combination of both shear strains that act in each of the octahedral planes, through

$$\varepsilon_{Mises} = \frac{3}{2\sqrt{2}\cdot(1+\bar{\nu})}\gamma_{Mises} = \frac{\sqrt{(\varepsilon_x-\varepsilon_y)^2+(\varepsilon_x-\varepsilon_z)^2+(\varepsilon_y-\varepsilon_z)^2+1.5(\gamma_{xy}^2+\gamma_{xz}^2+\gamma_{yz}^2)}}{\sqrt{2}\cdot(1+\bar{\nu})} \quad (3)$$

Since the ε_{Mises} (as well as the γ_{Mises}) equation is always positive, a Mises strain range $\Delta\varepsilon_{Mises}$ (also known as the relative Mises strain ε_{RMises}) should be used to evaluate its variation due to a change $(\Delta\varepsilon_x, \Delta\varepsilon_y, \Delta\varepsilon_z, \Delta\gamma_{xy}, \Delta\gamma_{xz}, \Delta\gamma_{yz})$ in the strain components along some loading path:

$$\Delta\varepsilon_{Mises} = \varepsilon_{RMises} = \frac{\sqrt{(\Delta\varepsilon_x-\Delta\varepsilon_y)^2+(\Delta\varepsilon_x-\Delta\varepsilon_z)^2+(\Delta\varepsilon_y-\Delta\varepsilon_z)^2+1.5(\Delta\gamma_{xy}^2+\Delta\gamma_{xz}^2+\Delta\gamma_{yz}^2)}}{\sqrt{2}\cdot(1+\bar{\nu})} \quad (4)$$

An octahedral (or Mises) shear range parameter $\Delta\gamma_{Mises}$ can also be defined, related to the Mises strain range by

$$\Delta\varepsilon_{Mises} = \frac{3\cdot\Delta\gamma_{Mises}}{2\sqrt{2}(1+\bar{\nu})} \quad (5)$$

Note that the octahedral stress or strain shear ranges $\Delta\tau_{Mises}$ or $\Delta\gamma_{Mises}$ are measured on the octahedral planes, they are not equal to twice the shear amplitudes τ_a or γ_a acting on the considered plane. But those shear amplitudes could be easily obtained by

$$\tau_a = \frac{\sqrt{6}}{4}\Delta\tau_{Mises} = \frac{\sqrt{3}}{6}\Delta\sigma_{Mises} \quad \text{and} \quad \gamma_a = \frac{\sqrt{3}}{6}\Delta\gamma_{Mises} = \frac{1+\bar{\nu}}{\sqrt{3}}\Delta\varepsilon_{Mises} \quad (6)$$

Finally, for the linear elastic case, all these relative Mises stresses and strains correlate with the Mises shear range parameters by

$$\Delta\sigma_{Mises} = E\cdot\Delta\varepsilon_{Mises} = \frac{3}{\sqrt{2}}\cdot\Delta\tau_{Mises} = \frac{3E}{2\sqrt{2}\cdot(1+\bar{\nu})}\cdot\Delta\gamma_{Mises} \quad (7)$$

3. REDUCED ORDER STRESS AND STRAIN SPACES

When dealing with incremental plasticity, it is convenient to represent the stresses or strains in a 9-dimensional (9D) space. In particular, when representing the deviatoric stress tensor in 9D, its norm $|\bar{S}|$ becomes directly proportional to the Mises stress and octahedral (or Mises) shear stress, namely $|\bar{S}| = \sigma_{Mises}\cdot\sqrt{6}/3 = \tau_{Mises}\cdot\sqrt{3}$. In addition, the Prandtl-Reuss flow rule results in slightly different (and probably better) equations when formulated in 9D space than the equations derived using a reduced 6-dimensional (6D) formulation.

But, to find effective ranges in VA-NP histories, it is a good idea to work in a space with reduced dimensions, saving computational effort without modifying the results. The reduction from 9D to 6D deviatoric stresses is simply a matter of eliminating the τ_{yx}, τ_{zx} and τ_{zy} components from the deviatoric stress tensor, which are redundant because $\tau_{yx} \equiv \tau_{xy}$, $\tau_{zx} \equiv \tau_{xz}$, and $\tau_{zy} \equiv \tau_{yz}$.

Since the deviatoric stresses S_x, S_y and S_z are linear-dependent, because $S_x + S_y + S_z = 0$, it is possible to further reduce the deviatoric stress dimension from 6D to 5D. There are infinite ways to do this, for example replacing the

stresses S_x, S_y and S_z by new variables $S_1 \equiv a_{x1} \cdot S_x + a_{y1} \cdot S_y + a_{z1} \cdot S_z$ and $S_2 \equiv a_{x2} \cdot S_x + a_{y2} \cdot S_y + a_{z2} \cdot S_z$, where the user-defined coefficients a_{x1}, a_{y1}, a_{z1}, a_{x2}, a_{y2} and a_{z2} are any values that make the vectors $[a_{x1}\ a_{y1}\ a_{z1}]^T$, $[a_{x2}\ a_{y2}\ a_{z2}]^T$, and $[1\ 1\ 1]^T$ become linear independent. A notable example of such transformation is the one proposed by Papadopoulos et al. [21], who chose $[a_{x1}\ a_{y1}\ a_{z1}]^T = [\sqrt{3}/2\ 0\ 0]^T$ and $[a_{x2}\ a_{y2}\ a_{z2}]^T = [0\ 0.5\ -0.5]^T$, resulting in a reduced-order deviatoric stress tensor $\overline{S}'$ represented in a 5D transformed Euclidean stress-space $E_{5\sigma}$, where

$$\begin{cases} \overline{S}' \equiv \left[S_1 \quad S_2 \quad S_3 \quad S_4 \quad S_5 \right]^T \\ S_1 \equiv \sigma_x - \dfrac{\sigma_y}{2} - \dfrac{\sigma_z}{2} = \dfrac{3}{2} S_x, \quad S_2 \equiv \dfrac{\sigma_y - \sigma_z}{2}\sqrt{3} = \dfrac{S_y - S_z}{2}\sqrt{3} \\ S_3 \equiv \tau_{xy}\sqrt{3}, \quad S_4 \equiv \tau_{xz}\sqrt{3}, \quad S_5 \equiv \tau_{yz}\sqrt{3} \end{cases} \tag{8}$$

The above defined 5D deviatoric stress $\overline{S}'$ has three very interesting properties:

1) the norm of the 5D vector $\overline{S}'$ from the $E_{5\sigma}$ transformed deviatoric stress-space is equal to the Mises equivalent stress σ_{Mises};
2) the Euclidean distance in the 5D $E_{5\sigma}$ stress-space between any 2 points $\overline{S}_A' = [S_{1A}\ S_{2A}\ S_{3A}\ S_{4A}\ S_{5A}]^T$ and $\overline{S}_B' = [S_{1B}\ S_{2B}\ S_{3B}\ S_{4B}\ S_{5B}]^T$, respectively associated with the 9D deviatoric stresses $\overline{S}_A$ and $\overline{S}_B$, is equal to the Mises stress range $\Delta\sigma_{Mises}$ between these stress states; and
3) the locus of the points which have the same $\Delta\sigma_{Mises}$ with respect to a point $\overline{S}'$ in the $E_{5\sigma}$ deviatoric stress-space is the surface of a hypersphere with center in $\overline{S}'$ and radius $\Delta\sigma_{Mises}$. This is a simple corollary from the second property.

Note that, for unnotched specimens under histories combining uniaxial tension σ_x and torsion τ_{xy}, the 5D deviatoric stress $\overline{S}'$ can be represented in the classical diagram $\sigma_x \times \tau_{xy}\sqrt{3}$ using the 2D projection $[S_1\ \ S_3]^T$, since in this case $S_1 = \sigma_x$, $S_3 = \tau_{xy}\sqrt{3}$, and $S_2 = S_4 = S_5 = 0$.

The above properties will be useful to obtain effective stress ranges. For strain histories, it is possible to define a similar transformation to a 5D transformed Euclidean strain-space $E_{5\varepsilon}$ for the deviatoric strains, resulting in a reduced-order deviatoric strain $\overline{e}'$ represented by

$$\begin{cases} \overline{e}' \equiv \left[e_1 \quad e_2 \quad e_3 \quad e_4 \quad e_5 \right]^T \\ e_1 \equiv \dfrac{3}{2} \cdot \dfrac{e_x}{1+\overline{\nu}} = \dfrac{2\varepsilon_x - \varepsilon_y - \varepsilon_z}{2 \cdot (1+\overline{\nu})}, \quad e_2 \equiv \dfrac{e_y - e_z}{2 \cdot (1+\overline{\nu})}\sqrt{3} = \dfrac{\varepsilon_y - \varepsilon_z}{2 \cdot (1+\overline{\nu})}\sqrt{3}, \\ e_3 \equiv \dfrac{\gamma_{xy}\sqrt{3}}{2 \cdot (1+\overline{\nu})}, \quad e_4 \equiv \dfrac{\gamma_{xz}\sqrt{3}}{2 \cdot (1+\overline{\nu})}, \quad e_5 \equiv \dfrac{\gamma_{yz}\sqrt{3}}{2 \cdot (1+\overline{\nu})} \end{cases} \tag{9}$$

where $\overline{\nu}$ is the effective Poisson coefficient.

The above defined deviatoric strain $\overline{e}'$ in the transformed strain-space $E_{5\varepsilon}$ also has three interesting properties, very similar to the ones from $\overline{S}'$:

1) the norm of the 5D vector $\overline{e}'$ in the $E_{5\varepsilon}$ strain-space is equal to the Mises equivalent strain ε_{Mises};
2) the Euclidean distance in the 5D $E_{5\varepsilon}$ strain-space between any 2 points $\overline{e}_A' = [e_{1A}\ e_{2A}\ e_{3A}\ e_{4A}\ e_{5A}]^T$ and $\overline{e}_B' = [e_{1B}\ e_{2B}\ e_{3B}\ e_{4B}\ e_{5B}]^T$, respectively associated with the 9D deviatoric strains $\overline{e}_A$ and $\overline{e}_B$, is equal to the Mises strain range $\Delta\varepsilon_{Mises}$ between these strain states; and
3) the locus of the points which have the same $\Delta\varepsilon_{Mises}$ with respect to a point $\overline{e}'$ in the E_{5e} deviatoric space is the surface of a hypersphere with center in $\overline{e}'$ and radius $\Delta\varepsilon_{Mises}$. This is a simple corollary from the second property.

Note that, in strain histories where the plastic deformations dominate, it is possible to estimate $\overline{\nu} \cong \nu_{pl} = 0.5$, resulting in $e_3 = \gamma_{xy}\sqrt{3}/(2+2\overline{\nu}) \cong \gamma_{xy}\sqrt{3}/3 = \gamma_{xy}/\sqrt{3}$, $e_4 = \gamma_{xz}/\sqrt{3}$ and $e_5 = \gamma_{yz}/\sqrt{3}$. However, note also that the common practice of representing strain histories in traction-torsion tests using an $\varepsilon_x \times [\gamma_{xy}/\sqrt{3}]$ diagram is only appropriate if the plastic strains are really dominant, otherwise the general definition using $\overline{\nu}$ should be used instead. In addition, such 2D diagram is only appropriate for uniaxial tension-torsion with $\sigma_y = \sigma_z = 0$ histories, which implies that $\varepsilon_y = \varepsilon_z = -\overline{\nu} \cdot \varepsilon_x$ and therefore $e_1 \equiv \varepsilon_x$, as proven next.

The above 5D deviatoric stresses and strains can represent any multiaxial history, even at points below the surface of the specimen. In the particular case of points at a free surface perpendicular to the *z* direction, the plane stress condition gives $\sigma_z = \tau_{xz} = \tau_{yz} = 0$ and $\gamma_{xz} = \gamma_{yz} = 0$, so the deviatoric stress and strain can be further reduced to 3D sub-spaces

$$\bar{S}'' = \left[S_1 \quad S_2 \quad S_3\right]^T, \text{ where } S_1 \equiv \sigma_x - \frac{\sigma_y}{2},\ S_2 \equiv \frac{\sigma_y}{2}\sqrt{3},\ S_3 \equiv \tau_{xy}\sqrt{3} \tag{10}$$

$$\bar{e}'' \equiv \left[e_1 \quad e_2 \quad e_3\right]^T, \text{ where } e_1 \equiv \frac{2\varepsilon_x - \varepsilon_y - \varepsilon_z}{2\cdot(1+\bar{\nu})},\ e_2 \equiv \frac{\varepsilon_y - \varepsilon_z}{2\cdot(1+\bar{\nu})}\sqrt{3},\ e_3 \equiv \frac{\gamma_{xy}\sqrt{3}}{2\cdot(1+\bar{\nu})} \tag{11}$$

Note that the plane stress equation $\varepsilon_z = -\nu\cdot(\varepsilon_x + \varepsilon_y)/(1-\nu)$ can only be used above for elastic strains. For elasto-plastic strain histories, ε_z must be calculated using e.g. incremental plasticity algorithms, or estimated from the effective Poisson coefficient, assuming $\varepsilon_Z \cong -\bar{\nu}\cdot(\varepsilon_X + \varepsilon_Y)/(1-\bar{\nu})$.

For surface stress histories consisting only of uniaxial tension σ_x and torsion τ_{xy} combinations (where $\sigma_y = \sigma_z = \tau_{xz} = \tau_{yz} = 0$), 2D sub-spaces can be used to represent the deviatoric stress and strain

$$\bar{S}''' = \left[S_1 \quad S_3\right]^T, \text{ where } S_1 \equiv \sigma_x,\ S_3 \equiv \tau_{xy}\sqrt{3} \tag{12}$$

$$\bar{e}''' \equiv \left[e_1 \quad e_3\right]^T, \text{ where } e_1 \equiv \frac{2\varepsilon_x + \bar{\nu}\varepsilon_x + \bar{\nu}\varepsilon_x}{2\cdot(1+\bar{\nu})} = \varepsilon_x,\ e_3 \equiv \frac{\gamma_{xy}\sqrt{3}}{2\cdot(1+\bar{\nu})} \tag{13}$$

where it was assumed that $\varepsilon_y = \varepsilon_z \cong -\bar{\nu}\cdot\varepsilon_x$, which results in $e_1 \equiv \varepsilon_x$ (as mentioned before) while making $e_2 \equiv 0$.

After defining all involved stress and strain parameters, the convex hull methods are discussed. These methods are based on convex hulls enclosing the history path in the above defined stress or strain sub-spaces. There are 3 types of convex hulls: balls, ellipsoids and rectangular prisms. The Minimum Ball method is presented next.

4. MINIMUM BALL METHOD

Dang Van (1999) realized that the search for an effective stress range must take place on the deviatoric stress space. For periodic elastic histories, the mesoscopic stresses and strains in the critically oriented grain should stabilize by the process of elastic shakedown, generating a local residual stress $[\sigma_{ij}]_{res}$ at such critical grain. Dang Van assumed that the subsequent mesoscopic (μ) stress history at such grain, after the stabilization, is related to the macroscopic (M) history through

$$[\sigma_{ij}(t)]_\mu = [\sigma_{ij}(t)]_M + dev[\sigma_{ij}]_{res} \tag{14}$$

where $dev[\sigma_{ij}]_{res}$ is the deviatoric part of the residual stresses tensor stabilized in that grain.

The calculation of the mesoscopic stresses in Dang Van's model can be interpreted as a hardening problem, caused by elastic shakedown. When the periodic macroscopic history is represented in the deviatoric space, Dang Van assumes that the stabilized residual stress is the vector from the center of the minimum ball that circumscribes the history to the origin of the diagram. The word "ball" is used here to describe a circle, sphere or hypersphere, respectively for 2D, 3D or higher dimension histories. The same result holds if the reduced stress $E_{5\sigma}$ (or strain $E_{5\varepsilon}$) space is used, or a sub-space from it.

The values of the mesoscopic Tresca stress $\tau_\mu(t)$ and mesoscopic hydrostatic stress $\sigma_{\mu h}(t)$ (which is equal to the macroscopic hydrostatic stress) are calculated for each point in the mesoscopic history path $\boldsymbol{D}_\mu$. Dang Van then predicts infinite life if and only if all points satisfy the inequality

$$\tau_\mu(t) + \alpha_{DV}\cdot\sigma_{\mu h}(t) \le \beta_{DV} \tag{15}$$

There are several algorithms to find the minimum radius circle (or sphere or hypersphere, for higher dimensions) that circumscribes the load history, such as the miniball method proposed by Gärtner (1999). This miniball method is an optimization of the work from Welzl (1991).

In summary, Dang Van is a type of Minimum Ball (MB) method where each stress state along the history path is compared to a limiting stress level to predict infinite life. However, it is not useful to calculate finite fatigue lives, since it does not deal with stress (or strain) ranges, only with individual stress states.

But the same MB circumscribed to the macroscopic history can be used to estimate an effective Mises stress range $\Delta\sigma_{Mises}$ (or strain range $\Delta\varepsilon_{Mises}$). The diameter d of such MB in the transformed deviatoric stress-space $E_{5\sigma}$ or strain-space $E_{5\varepsilon}$ (or in a 2D, 3D or 4D sub-space of such spaces) is the magnitude of the variation $\Delta\bar{S}'$ (or $\Delta\bar{e}'$), which is equal to $\Delta\sigma_{Mises}$ (or $\Delta\varepsilon_{Mises}$). Therefore, the effective shear ranges $\Delta\tau_{max}$ (used in the Findley and McDiarmid models)

and $\Delta\gamma_{max}$ (used in the Brown-Miller and Fatemi-Socie models), Mises ranges $\Delta\sigma_{Mises}$ and $\Delta\varepsilon_{Mises}$, and octahedral shear ranges $\Delta\tau_{Mises}$ (used in the Sines and Crossland models) and $\Delta\gamma_{Mises}$, can be estimated from d using the MB method by

$$\begin{aligned}\Delta\sigma_{Mises} &= 3\cdot\Delta\tau_{Mises}/\sqrt{2} = \Delta\tau_{max}\sqrt{3} = (2\tau_a)\cdot\sqrt{3} = |\Delta\bar{S}'| = d \equiv L\cdot\lambda_{MB} \quad \text{or} \\ \Delta\varepsilon_{Mises} &= 3\cdot\frac{\Delta\gamma_{Mises}}{2\sqrt{2}(1+\bar{\nu})} = \frac{\Delta\gamma_{max}\sqrt{3}}{2(1+\bar{\nu})} = \frac{(2\gamma_a)\cdot\sqrt{3}}{2(1+\bar{\nu})} = |\Delta\bar{e}'| = d \equiv L\cdot\lambda_{MB}\end{aligned} \tag{16}$$

where L is the longest chord in the history (the maximum Euclidean distance in the transformed space between any two points along the history path, measured in either stress or strain units), and λ_{MB} is a dimensionless parameter defined as the ratio between the Mises stress or strain range for the Minimum Ball method and such longest chord L. This ratio will be useful to compare the equivalent stresses and strains predicted by the different methods.

In the 2D case, if any two points from the history define the diameter of a circle that contains the entire path, then their distance L is equal to the diameter d, therefore the ratio becomes $\lambda_{MB} = 1.0$. A notable 2D case is for a path forming an equilateral triangle, where $\lambda_{MB} = 2/\sqrt{3} \cong 1.155$. For any other 2D path, it is found that $1.0 \le \lambda_{MB} \le 1.155$.

5. MINIMUM ELLIPSOID METHODS

The Minimum Ball (MB) method is not efficient to represent the behavior of NP histories. For instance, it would predict the same Mises ranges for a NP 90° out-of-phase circular path and a proportional path defined by a diameter of this circle, both resulting in $\lambda_{MB} = 1.0$. But a higher value of λ_{MB} would certainly be expected for the NP history.

To solve this problem, Freitas et al. (2000) proposed the Minimum Circumscribed Ellipsoid (MCE) method. It searches for an ellipse (or ellipsoid or hyperellipsoid, for higher dimensions) that circumscribes the entire history, with its longest semi-axis a_1 equal to the radius of the minimum ball, and with the smallest possible values for the remaining semi-axes a_i ($i > 1$). The Mises ranges are defined by

$$\Delta\sigma_{Mises} \quad \text{or} \quad \Delta\varepsilon_{Mises} = 2\cdot\sqrt{\sum_{i=1}^{dim} a_i^{\,2}} \equiv 2\cdot F \tag{17}$$

where dim is the dimension of the history path, $2 \le dim \le 5$, and F is defined as the Frobenius norm of the ellipsoid, which is equal to the square root of the sum of the squares of the ellipsoid semi-axes. Here, the Frobenius norm is essentially an Euclidean distance (or Euclidean norm) between the origin and a point with coordinates $(a_1, a_2, \ldots, a_{dim})$, since the axes of the reduced stress (or strain) space are orthonormal. In the case of tensors, the Euclidean norm is commonly called the Frobenius norm, usually abbreviated as F-norm.

The ratio between the Mises ranges calculated by the MCE method and the longest chord L, defined here as λ_{MCE}, reproduces experimental data better than λ_{MB} generated by the MB method. In the 2D case, a NP circular path would result in $\lambda_{MCE} = \sqrt{2}$ instead of the proportional value 1.0, which is much more reasonable than the Minimum Ball prediction. It is also found that any 2D path results in $1.0 \le \lambda_{MCE} \le \sqrt{2}$, with the maximum value occurring e.g. for circular and square paths. In general, for any dimension dim, it is found that $1.0 \le \lambda_{MCE} \le \sqrt{dim}$, with the maximum value $\sqrt{dim}$ occurring e.g. for paths that follow the edges of hypercubes or large portions of the surface of hyperspheres. The downside of the MCE method is the requirement that the longest semi-axis must be equal to the radius of the Minimum Ball.

A possible alternative to the MCE method is to search for the Minimum Volume Ellipsoid (MVE), also known as the Löwner-John Ellipsoid. In the 2D case, it is basically the search for an enclosing ellipse with minimum area. Such MVE method solves the MCE issues with rectangular paths, however it tends to find ellipses with lower aspect ratios than expected. In addition, the search for such ellipsoid or hyperellipsoid can be computationally intensive for 3D or higher dimension histories.

Another alternative to the MCE method is the search for the Minimum F-norm Ellipsoid (MFE) (Gonçalves et al., 2005). Instead of searching for the minimum volume (or area), the MFE looks for the ellipse, ellipsoid, or hyperellipsoid with minimum value of its F-norm F, defined in Eq. (17). Zouain et al. (2006) present an efficient (although computationally intensive) method to numerically find such MFE. Other efficient algorithms can be found in (Bernasconi, 2002).

The ratios between the Mises stress or strain ranges $2\cdot F$, calculated from the MCE, MVE and MFE methods, and the longest chord L are defined, respectively, as λ_{MCE}, λ_{MVE} and λ_{MFE}. All these ratios must be greater than or equal to 1.0. In the 2D case, a notable path is the one with the shape of an equilateral triangle with sides L (which are also its longest chords), where the resulting hull is a circle with diameter $d = 2L/\sqrt{3}$ and F-norm $F = d\sqrt{2}$, resulting in $\lambda_{MCE} = \lambda_{MVE} = \lambda_{MFE} = 2\cdot F/L = 2\sqrt{2}/\sqrt{3} \cong 1.633$. For any other 2D path, it is found that $1.0 \le \lambda_{MCE} \le 1.633$ and $1.0 \le \lambda_{MFE} \le 1.633$, however λ_{MVE} can reach values beyond 2.0 when a very elongated enclosing ellipse is the solution with minimum area, an indication that the MVE method can be very conservative.

6. MAXIMUM PRISMATIC HULL METHODS

Another class of convex hull methods tries to find a rectangular prism with sides $2a_1$, ..., $2a_{dim}$ that encloses a load history path, where *dim* is the dimension of the considered space. There are essentially 4 methods to fit rectangular prisms to the history path.

The first is the Maximum Prismatic Hull (MPH). This method searches for the smallest rectangular prism that encloses the history (the minimum prism), for each possible orientation of the prism. Among them, the one with highest F-norm is chosen. The F-norm and resulting Mises ranges are the same defined in Eq. (17), except that here a_i are the semi-lengths (half the length) of the sides of the rectangular prism. The MPH was originally proposed by Gonçalves et al. (2005) for sinusoidal time histories, and later extended by Mamiya et al. (2009) for a general NP loading.

Another prismatic hull method is the Maximum Volume Prismatic Hull (MVPH), which searches among the minimum prisms the one with maximum volume. Although the search is for a maximum volume, the F-norm is also used to compute the Mises range. In the 2D case, the MVPH method is essentially the search, among the minimum rectangles that enclose the entire path, of the one with maximum area (it's a max-min problem).

A third method is proposed here, called the Maximum Prismatic Hull with Longest Chords (MPHLC). It is basically an improvement of Deperrois' method (Deperrois, 1991). In the Deperrois method, the longest chord L_5 between any two points of the path in the projected 5D deviatoric stress-space $E_{5\sigma}$ (or deviatoric strain-space $E_{5\varepsilon}$, for strain histories) is determined. Then, the path is projected onto a 4D stress-subspace $E_{4\sigma}$ orthogonal to L_5, and the new longest chord L_4 is computed in this subspace. The path is then projected onto a stress-subspace $E_{3\sigma}$ orthogonal to both L_5 and L_4, and the new longest chord L_3 is computed in this subspace. Analogously, the longest chord L_2 is found in the stress-subspace $E_{2\sigma}$ orthogonal to L_5, L_4 and L_3. Finally, the longest chord L_1 is found in the stress-subspace $E_{1\sigma}$ orthogonal to L_5, L_4, L_3 and L_2.

The Deperrois method provides satisfactory results (Ballard et al., 1995). However, Papadopoulos et al. (1997) criticize it because, if any longest chord is non-unique, then different rectangular prisms and resulting shear amplitudes could be obtained for the same history. But this non-uniqueness could be easily solved by stating that, when the longest chords are non-unique, then the chosen prismatic hull would be the one with maximum F-norm among all possible results. The use of rectangular prisms with maximum F-norm has shown good results in the MPH method, therefore this could be the solution to Papadopoulos' criticisms.

The combination of the MPH and Deperrois' methods thus leads to the MPHLC method, performed in 4 steps:

1) define the longest side $2a_1$ of the rectangular prism in the direction of the longest chord L of the history;
2) project the history into the sub-space orthogonal to the directions of all sides of the prisms that have already been defined (for a history with dimension *dim*, if *m* sides have already been chosen, then such sub-space will have *dim*–*m* dimensions);
3) define the next side $2a_i$ of the rectangular prism in the direction of the longest chord measured in the projected sub-space, and repeat step 2 until all sides are found;
4) if multiple solutions for the rectangular prism are found, the one with maximum F-norm is chosen – this step addresses Papadopoulos' criticisms.

The advantage of the MPHLC method over the MPH or MVPH is that it does not require a numerical search for the prismatic hull orientation. Its orientation is deterministically defined by the longest chords. In special for 3D or higher dimension histories, the MPHLC method can lead to a huge decrease in computational effort. For instance, the orientation of a 5D hyperprism is given by 10 angles, therefore the search for the orientation associated with maximum F-norm (or maximum volume) involves a search in a 10-dimensional space, which can be very costly. In addition, the next sections will show that the MPHLC predictions give almost the same results as the MPH and MVPH methods.

A variation of the MPHLC is also proposed, called the Maximum Prismatic Hull with Container Chords (MPHCC). It is similar to the MPHLC, but all chords that contain the orthogonal projection of the entire history onto them (called here "container chords") are considered as candidate directions for the sides of the rectangular prism. Note that every longest chord LC is a "container chord" CC, but not every CC is a LC. From the probable multiple solutions for the resulting rectangular prisms, the one with maximum F-norm is chosen.

The ratios between the Mises stress or strain ranges $2 \cdot F$, calculated from the MPH, MVPH, MPHLC and MPHCC methods, and the longest chord L are defined, respectively, as λ_{MPH}, λ_{MVPH}, λ_{MPHLC} and λ_{MPHCC}. All these four ratios are, in average, very close to each other, therefore any of the four variations of the prismatic hull methods could be used interchangeably. For a history path with dimension *dim*, it is found that $1 \leq \lambda_{MPHLC} \leq \lambda_{MPHCC} \leq \lambda_{MPH} \leq \sqrt{dim}$, therefore the MPHCC results in Mises ratios slightly closer to the MPH predictions than the MPHLC. In addition, it is also found that $1 \leq \lambda_{MVPH} \leq \lambda_{MPH} \leq \sqrt{dim}$.

In the next section, all convex hull methods presented in this paper are evaluated and compared.

7. COMPARISON AMONG THE CONVEX HULL METHODS

Figure 3 shows the convex hulls obtained from all presented methods for a rectangular history path in a reduced 2D sub-space, and their ratios λ between the Mises ranges and longest chord L. Note that, in this example, L is the diagonal of the rectangular path.

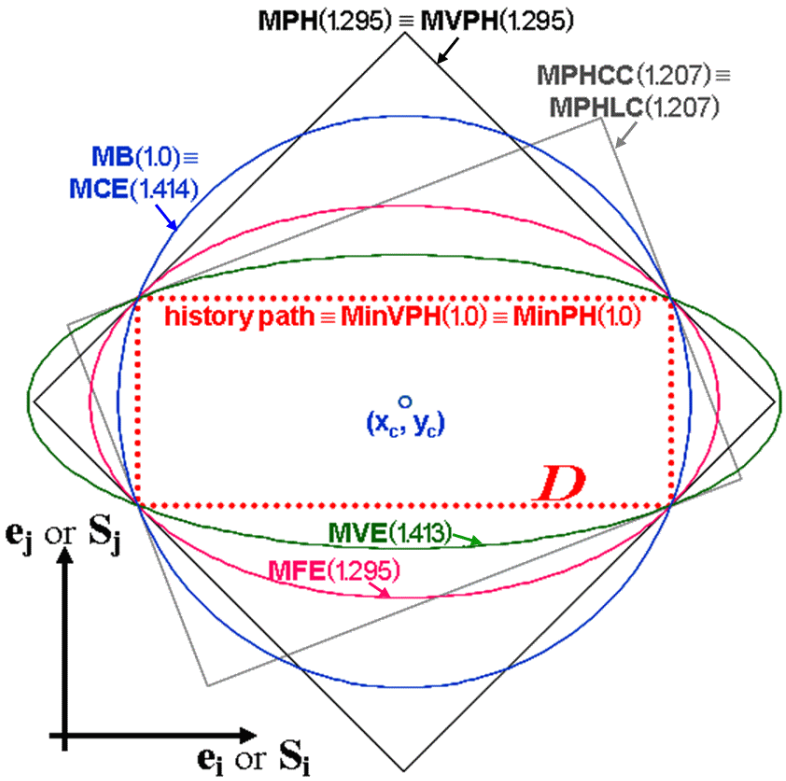

Fig. 3: Values of the λ Mises stress or strain range ratio for the MB, MCE, MVE, MFE, MPH, MPHLC, MPHCC, MVPH, MinPH and MinVPH methods for a rectangular 2D history path.

Experimental results suggest that the expected ratio λ in this example is about 1.3. However, the MB method predicts $\lambda_{MB} = 1.0$, which is very non-conservative. The MB assumes that such rectangular path would have the same Mises range L as a straight path along one of its diagonals, which is not reasonable. The MCE method, on the other hand, overestimates λ, obtaining $\lambda_{MCE} = \sqrt{2} \cong 1.414$. The MCE method finds the same circle from the MB to enclose such history, even though the aspect ratio of this rectangular path is very different from *1.0*, suggesting instead the use of an elongated elliptic hull.

The MVE method also tends to overestimate λ, obtaining in this example $\lambda_{MVE} = 1.413$. In the search for the minimum area (or volume, for higher dimension diagrams), the MVE method ends up finding overly elongated ellipses ($b << a$), which have a small area $\pi \cdot a \cdot b$ due to the very low value of b but an unrealistically high F-norm $(a^2+b^2)^{1/2}$ due to the high value obtained for a. Thus, λ_{MVE} overestimates the ratio λ, since it is calculated from this unrealistic F-norm, and not from the area (or volume).

Among the ellipsoid hull methods, the MFE gives the best predictions, resulting in $\lambda_{MFE} = 1.295$, with an enclosing ellipse with a much more reasonable aspect ratio than the ones from the MCE and MVE methods, see Fig. 3.

Both MPH and MVPH methods obtain in this example $\lambda_{MPH} = \lambda_{MVPH} = 1.295$, which exactly agrees with the MFE prediction. Note however that the MPH and MFE methods are not equivalent, since they result in slightly different λ values between them for other history paths, as shown in (Castro et al., 2009).

The MPHLC and MPHCC result in $\lambda_{MPHLC} = \lambda_{MPHCC} = 1.207$, a value about *7%* lower than the MPH prediction. The fact that $\lambda_{MPHLC} \leq \lambda_{MPH}$ and $\lambda_{MPHCC} \leq \lambda_{MPH}$ is not a surprise, since the MPH searches for the maximum F-norm checking rectangles (in the 2D case) in all directions, while the MPHLC and MPHCC only search for rectangles in the directions of the longest and/or container chords. If these directions of longest or container chords coincide with the ones associated with a maximum F-norm rectangle (which is quite often true), then the MPHLC or MPHCC predictions will coincide with λ_{MPH}, otherwise they will result in λ ratios slightly lower than the upper bound λ_{MPH}.

Figure 3 also shows the prismatic hulls MinPH and MinVPH with minimum (instead of maximum) F-norm and volume (or area, in 2D), respectively. In this example, these rectangular hulls would coincide with the original rectangular path, wrongfully predicting $\lambda = 1$. This counter-example shows why no prismatic hull method with minimum F-norm or volume has been proposed.

In summary, the MB method tends to underestimate the Mises stress or strain range ratio λ, while the MCE and MVE overestimate it. The MPHLC and MPHCC slightly underestimate λ, while the MFE, MPH and MVPH give very similar (although, in general, different) predictions.

But the above considerations are based on a single example. To really compare all convex hull methods, it is necessary to study all possible history path topologies in 2D, 3D, 4D and 5D deviatoric stress or strain spaces. Monte Carlo simulations are performed for $3 \cdot 10^6$ random 2D history paths, in addition to a few selected paths to try to cover all possible path topologies. All convex hull methods are applied to each of these simulated paths, to evaluate and compare the λ predictions.

The λ ratios estimated from the MPH and MPHCC methods are compared for the $3 \cdot 10^6$ Monte Carlo simulations. It is found that the MPHCC tends to underestimate λ when compared to the MPH, as expected. However, the differences are small: for 2D paths, in average, λ_{MPHCC} is about *98%* of λ_{MPH}, with a standard deviation of only *2.1%*. And, even for such rare paths, λ_{MPHCC} never underestimates λ_{MPH} by more than *10%*. In addition, the MPHLC and MPHCC usually give almost identical results, with λ_{MPHLC} being in average about *99.85%* of λ_{MPHCC}, with a standard deviation of only *0.9%* for these $3 \cdot 10^6$ simulations.

Similar conclusions apply to 3D, 4D and 5D load history paths in deviatoric stress or strain spaces, also obtained from Monte Carlo simulations. Note that fewer simulations were performed as the dimension increased, because of time restrictions, since most convex hull methods are very computationally intensive in higher dimensions. E.g., the search for the direction of a 5D hyperprism in the MPH method involves a search in a 10-dimensional space for the 10 angles that define its 5D orientation, which can take several seconds to be found in a typical personal computer, even for rough discretizations of each angle at 15^o steps. On the other hand, the MPHLC and MPHCC methods are straightforward, deterministic (no numerical search method based on discretizations is required) and several orders of magnitude faster, taking anything from a few microseconds to a few milliseconds to be calculated, depending on the size of the set of points that define the history path. These calculations are much faster and still result in the same MPH prediction for the Mises stress or strain range ratio λ within 2% (in average).

The $3 \cdot 10^6$ Monte Carlo 2D simulations are now used to compare the other convex hull methods. The MPH and MVPH are found to have a very good agreement, except for low values of λ. In addition, $\lambda_{MVPH} \leq \lambda_{MPH}$ and, in average, λ_{MVPH} is about *98.6%* of λ_{MPH}, with a standard deviation of only *1.8%*. Similar conclusions are found for 3D, 4D and 5D histories.

Let's now compare the MPH and MFE methods in 2D. Even though these methods seem coherent, they can lead to very different λ predictions. It is found that $\lambda_{MFE} \geq \lambda_{MPH}$ and, in average, λ_{MPH} is about *92.9%* of λ_{MFE}, with a standard deviation of *4.3%*. Similar conclusions are found for 3D, 4D and 5D histories. Note that the pair $(\lambda_{MPH}, \lambda_{MFE}) = (0.5 + \sqrt{3}/2 \cong 1.366, 2\sqrt{2}/\sqrt{3} \cong 1.633)$ denotes the (extreme) case of a path with the shape of an equilateral triangle. This significant difference between λ predictions suggests that a path shaped like an equilateral triangle would provide a very good discriminant experiment to compare the adequacy of the MPH and MFE methods for a certain material.

Now, let's compare the MPH and MVE methods in 2D. The MVE method can severely (and wrongfully) overestimate λ, in special for low values of λ_{MPH}, associated with almost proportional paths. As discussed before, almost proportional paths can lead to overly elongated ellipses in the MVE method, which can have a small area but an unrealistically large F-norm, leading to λ_{MVE} values larger than 2.0 in some extreme cases. Similar conclusions are found for 3D, 4D and 5D histories.

When the MFE and MCE methods are compared in 2D, it is found that λ_{MCE} overestimates λ, in special for low values of λ_{MFE}, associated with almost proportional paths. For instance, for an almost proportional history defined by a rectangular path with very low aspect ratio, the expected λ would be close to *1.0* (which is the expected value of λ for proportional histories), however the MCE method would circumscribe a circle (instead of an elongated ellipse) to such elongated rectangular path, wrongfully predicting $\lambda_{MCE} = \sqrt{2}$. An almost proportional triangular path would also result in this same notable pair $(\lambda_{MFE}, \lambda_{MCE}) = (1, \sqrt{2})$, revealing the inadequacy of the MCE method. Similar conclusions are found for 3D, 4D and 5D histories.

Comparing the MFE and MB methods in 2D, it is found that the MB method can severely (and wrongfully) underestimate λ, except for almost proportional load histories (where $\lambda_{MB} \cong \lambda_{MFE} \cong 1.0$). Good discriminant experiments to confirm the inadequacy of the MB method could make use of a square or circular path, where $(\lambda_{MFE}, \lambda_{MB}) = (\sqrt{2}, 1)$, or a path shaped as an equilateral triangle, where $(\lambda_{MFE}, \lambda_{MB}) = (2\sqrt{2}/\sqrt{3} \cong 1.633, 2/\sqrt{3} \cong 1.155)$. Both cases would result in $\lambda_{MFE}/\lambda_{MB} = \sqrt{2}$, a *41%* difference that could be easily verified experimentally. Similar conclusions are found for 3D, 4D and 5D histories.

Table 1 summarizes the medians of the ratios between the λ parameters from each model pair, as well as the coefficient of variation (COV) of such ratios. The medians are less influenced by the extreme values than the means.

Table 1: Median values of the ratios between the λ calculated using the models from each row and column from the table. The values in parentheses are the coefficient of variation (COV) of such ratios/correlations.

row / col	MPHLC	MPHCC	MPH	MVPH	MFE	MVE	MB	MCE
MPHLC	-	1.00 (0.9%)	0.98 (2.3%)	1.00 (3.4%)	0.91 (5.9%)	0.84 (7.7%)	1.06 (6.2%)	0.87 (8.8%)
MPHCC	1.00 (0.9%)	-	0.98 (2.1%)	1.00 (3.2%)	0.91 (5.7%)	0.84 (7.7%)	1.06 (6.3%)	0.87 (8.6%)
MPH	1.02 (2.3%)	1.02 (2.2%)	-	1.01 (1.9%)	0.93 (4.3%)	0.86 (6.6%)	1.09 (6.9%)	0.88 (7.0%)
MVPH	1.00 (3.5%)	1.00 (3.3%)	0.99 (1.8%)	-	0.91 (4.3%)	0.85 (6.7%)	1.07 (7.8%)	0.86 (6.8%)
MFE	1.10 (5.9%)	1.10 (5.7%)	1.08 (4.3%)	1.10 (4.3%)	-	0.95 (6.5%)	1.18 (10.4%)	0.97 (4.1%)
MVE	1.19 (7.7%)	1.19 (7.7%)	1.16 (6.8%)	1.17 (6.9%)	1.05 (7.7%)	-	1.28 (8.8%)	1.00 (9.2%)
MB	0.94 (5.7%)	0.94 (5.8%)	0.92 (6.6%)	0.93 (7.4%)	0.85 (10.2%)	0.78 (9.6%)	-	0.80 (12.9%)
MCE	1.15 (8.7%)	1.15 (8.6%)	1.13 (6.9%)	1.16 (6.4%)	1.03 (4.5%)	1.00 (7.6%)	1.25 (12.2%)	-

8. CONCLUSIONS

In this work, all convex hull methods from the literature were reviewed and compared, and new methods were proposed. The conclusions from the comparisons are:

1. the prismatic hull methods MPHLC and MPHCC are very similar to the MPH and MVPH methods, but with a much simpler search algorithm for 3D to 5D histories;
2. the only recommended ellipsoid hull is the Minimum F-norm Ellipsoid (MFE), which results in similar (but not equal) λ predictions when compared to the prismatic hull methods; and
3. the Minimum Circumscribed Ellipsoid (MCE), Minimum Volume Ellipsoid (MVE), and Minimum Ball (MB) methods may result in very poor predictions of the stress or strain amplitudes.

In summary, the Minimum F-norm Ellipsoid and all four Maximum Prismatic Hull (MPH) models are efficient to predict equivalent amplitudes in NP histories.

9. ACKNOWLEDGEMENTS

CNPq has provided research scholarships for the authors.

10. REFERENCES

Ballard, P., Dang Van, K., Deperrois, A., Papadopoulos, I.V., High Cycle Fatigue and a Finite Element Analysis, Fatigue Fract. Engng. Mater. Struct v.18, n.3, pp.397-411, 1995.

Bernasconi, A., Efficient algorithms for calculation of shear stress amplitude and amplitude of the second invariant of the stress deviator in fatigue criteria applications, International Journal of Fatigue, v.24, n.6, pp.649-657, 2002.

Castro, F.C., Araújo, J.A., Mamiya, E.N., Zouain, N., Remarks on multiaxial fatigue limit criteria based on prismatic hulls and ellipsoids, International Journal of Fatigue, v.31, pp.1875–1881, 2009.

Dang Van, K., Papadopoulos, I.V., High-Cycle Metal Fatigue. Springer 1999.

Deperrois, A., Sur le calcul des limites d'endurance des aciers. Thèse de Doctorat. Ecole Polytechnique, Paris, 1991.

Freitas, M., Li, B., Santos, J.L.T., Multiaxial Fatigue and Deformation: Testing and Prediction, ASTM STP 1387, 2000.

Gärtner, B., Fast and Robust Smallest Enclosing Balls, Proc. 7th Annual European Symposium on Algorithms (ESA), Lecture Notes in Computer Science 1643, Springer-Verlag, pp.325-338, 1999.

Gonçalves, C.A., Araújo, J.A., Mamiya, E.N., Multiaxial fatigue: a stress based criterion for hard metals, International Journal of Fatigue v.27, pp.177-187, 2005.

Langlais, T.E., Vogel, J.H., Chase, T.R., Multiaxial cycle counting for critical plane methods, International Journal of Fatigue 25, pp.641–647, 2003.

Mamiya, E.N., Araújo, J.A., Castro, F.C., Prismatic hull: A new measure of shear stress amplitude in multiaxial high cycle fatigue, International Journal of Fatigue, v.31, pp.1144-1153, 2009.

Papadopoulos, I.V., Davoli, P., Gorla, C., Filippini, M., Bernasconi, A., "A comparative study of multiaxial high-cycle fatigue criteria for metals", Int. Journal of Fatigue v.19, pp.219–235, 1997.

Socie, D.F., Marquis, G.B. Multiaxial Fatigue, SAE 1999.

Welzl, E., Smallest enclosing disks (balls and ellipsoids), New Results and New Trends in Computer Science, Springer, 1991.

Zouain, N., Mamiya, E.N., Comes, F., Using enclosing ellipsoids in multiaxial fatigue strength criteria, European Journal of Mechanics - A, Solids, v.25, pp. 51-71, 2006.

11. RESPONSIBILITY NOTICE

The authors are the only responsible for the printed material included in this paper.